A&A 506, 1071–1082 (2009)
DOI: 10.1051/0004-6361/200811601

Astronomy & Astrophysics

The bright galaxy population of five medium redshift clusters

II. Quantitative galaxy morphology

B. Ascaso[1,3], J. A. L. Aguerri[2], M. Moles[3], R. Sánchez-Janssen[2], and D. Bettoni[4]

[1] Department of Physics, University of California, Davis, One Shields Avenue, Davis, CA 95616, USA
e-mail: ascaso@physics.ucdavis.edu
[2] Instituto de Astrofísica de Canarias, C/ Vía Láctea, S/N, La Laguna, Spain
e-mail: jalfonso@iac.es, ruben@iac.es
[3] Instituto de Astrofísica de Andalucia, Camino Bajo de Huetor 50, 18008 Granada, Spain
e-mail: moles@iaa.es
[4] INAF – Osservatorio Astronomico di Padova, Vicolo Osservatorio 5, 35122 Padova, Italy
e-mail: daniela.bettoni@oapd.inaf.it

Received 29 December 2008 / Accepted 2 July 2009

ABSTRACT

Aims. Following the study presented in our previous paper, based on the Nordic Optical Telescope (NOT) sample, which consists of five clusters of galaxies within the redshift range $0.18 \leq z \leq 0.25$ imaged in the central 0.5–2 Mpc in very good seeing conditions, we have studied the quantitative morphology of their bright galaxy population
Methods. We analyzed the surface brightness profiles of the galaxy population in those clusters, after performing simulations in order to check the reliability of the fits. We also derived a quantitative morphological classification.
Results. The structural parameters derived from these analyses are presented. We obtained that the structural parameters of E/S0 galaxies are similar to those shown by galaxies in low redshift clusters. However, the disc scales are different. In particular, the scales of the discs of galaxies in medium redshift clusters are statistically different than those located in similar galaxies in the Coma cluster. However, the scales of the discs of galaxies in medium redshift clusters are similar to nearby field galaxies.
Conclusions. Our results suggest that the evolution of the disc component of galaxies in clusters is faster than in field ones. Mechanisms like galaxy harassment showing timescales of ∼1 Gyr could be responsible for this disc scale evolution. This indicates that spiral galaxies in clusters have undergone a strong evolution in the last 2.5 Gyr or that Coma is in some way anomalous.

Key words. galaxies: clusters: general – galaxies: structure – cosmology: observations

1. Introduction

The brightest galaxies in the central part of clusters of galaxies have been an object of study for many years (Kormendy 1977; Dressler 1980; Merritt 1984; Caon et al. 1993; Jørgensen & Franx 1994; Kauffmann et al. 1994; Bower et al. 1998; Fasano et al. 2000; Aguerri et al. 2004; De Lucia & Blaizot 2007; Ascaso et al. 2008). Most of these studies have investigated their link with the formation of their host halo, leading to two main scenarios: the monolithic (Merritt 1984; Bower et al. 1998) and the hierarchical (Kauffmann et al. 1994; De Lucia & Blaizot 2007). The former assumes the cluster to be formed first and, consequently, the galaxies do not undergo transformation after the cluster collapse. The latter, on the other hand, implies that the galaxies were formed earlier than the cluster and therefore, environmental effects or interacting mechanisms such as harassment (Moore et al. 1996), gas-stripping (Gunn & Gott 1972; Quilis et al. 2000), starvation (Bekki et al. 2002), or merging (Aguerri et al. 2001; Eliche-Moral et al. 2006) are able to alter the galaxy population.

The galaxy population has a bimodal nature based on its stellar population and the shape of its surface brightness profiles. As Driver et al. (2006) showed, the redder and more compact objects are usually early-type systems, while the late-type galaxies are, generally, bluer and less concentrated profiles. Recent results (Ascaso 2008; Bell 2008; Skibba et al. 2009; Cameron & Driver 2009) have pointed out that this bi-modal behaviour for field and cluster galaxies can be translated in the color-log(n) plane, where n is the Sérsic index (Sérsic 1968), up to redshift 1. This result agrees with the hierarchical clustering scenario, as the late type galaxy population would be formed by cooling the gas in the dark matter halos and, as a consequence, the early type population would be formed by merging of late type galaxy members or by dry-merging of the early type galaxies.

Many works related to the evolution of the galaxy population in clusters of galaxies have also shown a decrease of the S0/E fraction with redshift. This decrement is mainly due to the variation with redshift of the S0 fraction, while the elliptical fraction remains constant up to $z \sim 0.8$ (Fasano et al. 2000; Dressler et al. 1997; Postman et al. 2005; Desai et al. 2007). This fact indicates a different time scale for the process of formation of elliptical and lenticular galaxies. However, Jørgensen & Franx (1994) studied the nature of elliptical and S0 galaxies in the Coma cluster, suggesting that they are a continuum class of

Table 1. The sample of clusters.

Name	α(2000)			δ(2000)			z	#Frames	Area (Mpc^2)	Seeing ($''$)
A 2658	23	44	49	–12	17	39	0.185	1	0.3055	0.70
A 1643	12	55	54	+44	05	12	0.198	2	0.6810	0.55
A 1878	14	12	52	+29	14	28	0.220	2	0.7894	0.70
A 2111	15	39	40	+34	25	27	0.229	2	0.8030	0.70
A 1952	14	41	03	+28	37	00	0.248	2	0.7989	0.55–0.80

objects in their distribution of bulge-to-disk ratios. Subsequent studies have given support to this fact (Jørgensen et al. 1996; Krajnović et al. 2008).

Likewise, a number of papers reflect a continuity in the parameter space for bright elliptical and dwarf galaxies in clusters, (Sandage & Visvanathan 1978; Graham 2003; Gutiérrez et al. 2004; Aguerri et al. 2004; Ascaso et al. 2008) suggesting that these objects could be a continous family. However, recent studies have been devoted to the study of the physical differences between elliptical and spheroidal or dwarf elliptical galaxies (Aguerri et al. 2005; Aguerri & González-García 2009; Kormendy et al. 2009) suggesting recent evolution in their structural parameters. For example, Kormendy et al. (2009) have shown that the bright ($M_{VT} \leq -21.66$) elliptical galaxies in the Virgo cluster have cuspy cores, rotate slowly, have anisotropic velocity distributions, boxy isophotes and Sérsic values, n, larger than 4, while the faint ellipticals ($-21.54 \leq M_{VT} \leq -15.53$) do not have cores, rotate much faster, usually have more isotropic velocity distributions, disky isophotes and smaller Sérsic parameters. In addition, they confirm that the biggest elliptical galaxies have X-ray emitting gas whereas the smallest ones have a lack of it. Therefore, larger samples of faint dwarf galaxies at medium-high redshift is necessary to study their evolution.

The galaxy surface brightness and main structural parameters have been studied in several works for different samples. These samples have been restricted to local clusters (Caon et al. 1993; Jørgensen & Franx 1994; Aguerri et al. 2004; Gutiérrez et al. 2004) or to galaxy samples preselected by morphological type, (e.g. early types Caon et al. 1993; Jørgensen & Franx 1994; Graham 2003 or late types De Jong 1996; Graham 2001, 2003; Möllenhoff 2004). In addition, larger samples of field galaxies have been analyzed. For example, Trujillo & Aguerri (2004) presented quantitative structural parameters in the V-band rest-frame for all galaxies with $z < 1$ and $I814(AB) < 24.5$ mag in the Hubble Deep Fields North and South. Nevertheless, the present number of works devoted to the study of global samples of galaxies in clusters at medium redshift range is small (Fasano et al. 2000; Trujillo et al. 2001; Balogh et al. 2002). In this work, we have studied the surface brightness of the whole galaxy population in a sample of clusters of galaxies at medium redshift.

Our data consists of five clusters observed with the Nordic Optical Telescope (NOT) in very good seeing conditions with two filters in a range of redshift from 0.18 to 0.25, where there are very few cases of clusters analysed due to difficulties in the deepness and quality of the observations. The analysis of the properties of such clusters can provide a new perspective on the evolutionary trends of clusters at that range of redshift, as well as the extension of the properties of other samples at low redshift to high redshift (HST).

In this paper, we have continued the analysis of the properties of the brightest galaxies ($m_r \leq 20$) in the central part of this cluster sample at medium redshift. We have analyzed their surface brightness, and performed a study of their structural parameters. We have also extracted their quantitative morphology and compared this to their visual morphology already derived in Ascaso et al. (2008).

The structure of this paper is as follows. In Sect. 2, we describe our sample and its analysis and we explain how we have fitted the surface brightness analysis to a one-Sérsic profile (Sérsic 1968) or a two-component, Sérsic+ exponential profile (Freeman 1970). In Sect. 3, we explain and show the results of the simulations for the establishment of the range of the parameters where we can fit the different models. In Sect. 4, we describe the galaxy classification and analyze the structural parameters extracted from the surface brightness fits for bulge and disc galaxies. A discussion of the results and conclusions are given in Sect. 5. The color figures are available electronically. Throughout that paper we have adopted a ΛCDM cosmology: $H_0 = 71$ km s^{-1} Mpc^{-1}, $\Omega_m = 0.27$ and $\Omega_\Lambda = 0.73$.

2. Data analysis

We have extended our study to the data previously presented in Ascaso et al. (2008) of five clusters of galaxies imaged with the Stand Camera of the 2.5 m Nordic Optical Telescope (NOT) located at the Roque de Los Muchachos Observatory (La Palma). The main characteristics of the sample are collected in Table 1.

We refer the reader to Fasano et al. (2000) for more extended details about the observations and the data reduction process. The detection and extraction of the galaxy sample is explained in Ascaso et al. (2008).

2.1. Two dimensional surface brightness fit

The surface brightness of the galaxies in our medium redshift clusters were modelled using one or two photometric components. The fits were carried out using the automatic fitting routine (GASP-2D) developed and successfully validated by Méndez-Abreu et al. (2008). The surface brightness of those galaxies modelled with only one component was described by a Sérsic law (Sérsic 1968), while the surface brightness of those galaxies fitted with two photometrical components was described by a Sérsic law plus an exponential (Freeman 1970).

The fits of the galaxies were fully two-dimensional. The photometric galaxy components were characterized by elliptical and concentric isophotes with constant (but possibly different) ellipticity and position angle. We have assumed a Cartesian coordinate system (x, y, z) with the origin in the galaxy center, the x-axis parallel to the direction of the right ascension and pointing westward, the y-axis parallel to the direction of declination and pointing northward, and the z-axis along the line-of-sight and pointing toward the observer. The plane of the sky is confined to the (x, y) plane, and the galaxy center is located at the position (x_0, y_0).

The Sérsic law has been extensively used in the literature to model the surface brightness of elliptical galaxies (Graham & Guzman 2003; Graham & Driver 2005), bulges of early and late-type galaxies, (Andredakis et al. 1995; Prieto et al. 2001; Aguerri et al. 2004; Möllenhoff 2004), the low surface brightness host of blue compact galaxies (Caon et al. 2005; Amorin et al. 2007; Amorín et al. 2009), and dwarf elliptical galaxies (Binggeli & Jerjen 1998; Graham & Guzman 2003; Aguerri et al. 2005). The radial variation of the intensity of this law is given by:

$$I(r) = I_{\rm e} 10^{-b_n[(r/r_{\rm e})^{1/n}-1]} \quad (1)$$

where $r_{\rm e}$, $I_{\rm e}$, and n are the effective radius, the intensity at $r_{\rm e}$ and a shape parameter, respectively. The value of $b_n = 0.868n - 0.142$ is coupled to n so that half of the total luminosity is within $r_{\rm e}$, (see Caon et al. 1993). The isophotes of the Sérsic models are concentred ellipses centred at (x_o, y_o) with constant position angle PA_b and constant ellipticity $\epsilon_b = 1 - q_b$. Thus, the radius r_b is given by:

$$r_b = [(-(x-x_o)\sin \mathrm{PA}_b + (y-y_o)\cos \mathrm{PA}_b)^2 - ((x-x_o)\cos \mathrm{PA}_b + (y-y_o)\sin \mathrm{PA}_b)^2/q_b^2]^{1/2}. \quad (2)$$

Hereafter, we will call "bulge" the photometric galaxy component fitted by a Sérsic law in those galaxies fitted with two components.

On the other hand, the exponential law has been used in the literature to model the surface brightness profile of the discs shown by spiral galaxies (e.g. Aguerri et al. 2005 and references therein). This law was proposed by Freeman (1970) and is given by:

$$I(r) = I_0 \mathrm{e}^{-r_d/h} \quad (3)$$

where I_0 and h are the central intensity and scale length, respectively. Similar to the photometric component modelled by a Sérsic law, we have considered that the disc isophotes are ellipses centered on the galaxy center (x_0, y_0) with constant position angle PA_d and constant ellipticity $\epsilon_d = 1 - q_d$, given by the galaxy inclination $i = \arccos(q_d)$. Thus, the radius r_d is given by:

$$r_d = [(-(x-x_0)\sin \mathrm{PA}_d + (y-y_0)\cos \mathrm{PA}_d)^2 - ((x-x_0)\cos \mathrm{PA}_d + (y-y_0)\sin \mathrm{PA}_d)^2/q_d^2]^{1/2}. \quad (4)$$

The GASP-2D routine fits all free parameters iteratively using a non-linear least-squares minimization method. It was based on the robust Levenberg-Marquardt method (Press et al. 1992). During each iteration of the fitted algorithm, the seeing effect was taken into account by convolving the model image with a circular point spread function (PSF) extracted from the images (see Méndez-Abreu et al. 2008, for more details about the fitting routine).

As many authors have recently explored, (Gadotti 2008; Cameron & Driver 2009), the presence of bars in the galaxies may result in poor bulge fits if not correctly modelled. Nevertheless, we address this by carefully examining the residuals.

3. Simulations

One of the advantages of the quantitative morphology is that the accuracy of the obtained results can be tested by simulating artificial galaxies similar to the real ones. We have created a large number of artificial galaxies with one and two galactic components described by the previous equations. These modeled galaxies are similar to the galaxies observed in our medium redshift galaxy clusters.

We generated 5000 images of galaxies with a Sérsic component. The total magnitude, effective radius, shape Sérsic parameter, and ellipticity of the simulated galaxies were similar to those from real galaxies. They were asigned randomly to the models, and their values were in the ranges:

$$18 \leq m_{\rm r} \leq 21; \quad 0.5 \text{ kpc} \leq r_{\rm e} \leq 4 \text{ kpc};$$

$$0.5 \leq n \leq 6; \quad 0.3 \leq q_b \leq 1 \quad (5)$$

We have also generated 5000 galaxies with two photometric components: Sérsic and exponential. These artificial galaxies have a central photometric "bulge" component, modeled by a Sersic law, and an external "disc" component, modeled by an exponential law. The total magnitude of these galaxies spans $18 \leq m_{\rm r} \leq 21$. The contribution to the total light of the galaxies by the bulge and disc components is given by the bulge-to-total light ratio. This parameter spreads over the range $0 \leq B/T \leq 1$. The bulge parameters of the simulated galaxies were:

$$0.5 \text{ kpc} \leq r_{\rm e} \leq 4 \text{ kpc}; \quad 0.5 \leq n \leq 6; \quad 0.2 \leq q_b \leq 1. \quad (6)$$

The disc free parameters of the galaxies were:

$$1.75 \text{ kpc} \leq h \leq 7 \text{ kpc}; \quad 0.2 \leq q_d \leq 1. \quad (7)$$

In order to mimic the same instrumental setup, we added a background level and photon noise to these artificial images similar to the observed images. They were also convolved simulating the seeing that we have in our observations. Finally, these simulated galaxies were fitted with the same conditions as the real ones. The simulated galaxies will be used to determine the errors of the fitted structural parameters.

3.1. Galaxies with one photometric component

Figure 1 shows the errors of the free parameters of those simulated galaxies with only one component as a function of their magnitude absolute errors for $\mu_{\rm e}$ and relative errors for $r_{\rm e}$, n and ϵ_b. Notice that bright galaxies show smaller relative errors in the fitted parameters than faint ones. Consequently, the goodnes of the fit depends on the galaxy magnitudes or, due to the correlation between area and magnitude, on the galaxy area. The areas of the objects were computed as the number of pixels with signal higher than 1.5 times the rms of the sky background of the images, and belonging to the intersection of the observed image and the fitted model. The last restriction was imposed in order to avoid wrong area measurements due to nearby objects.

We have considered that a galaxy was properly fitted when all free parameters were recovered with relative errors of less than 20%. Figure 2 shows the fraction of properly fitted simulated galaxies as a function of the area. We defined the minimum area of properly fitted galaxies as the one at which the fraction shown in Fig. 2 is equal to 0.5. This corresponds to 550 pixels for galaxies modeled with only one Sérsic component. This means that more than 50% of the galaxies with areas larger than 550 pixels were properly fitted.

3.2. Galaxies with two photometric components

Figure 4 shows the relative errors of the fitted free parameters of the simulated galaxies with bulge and disc components except

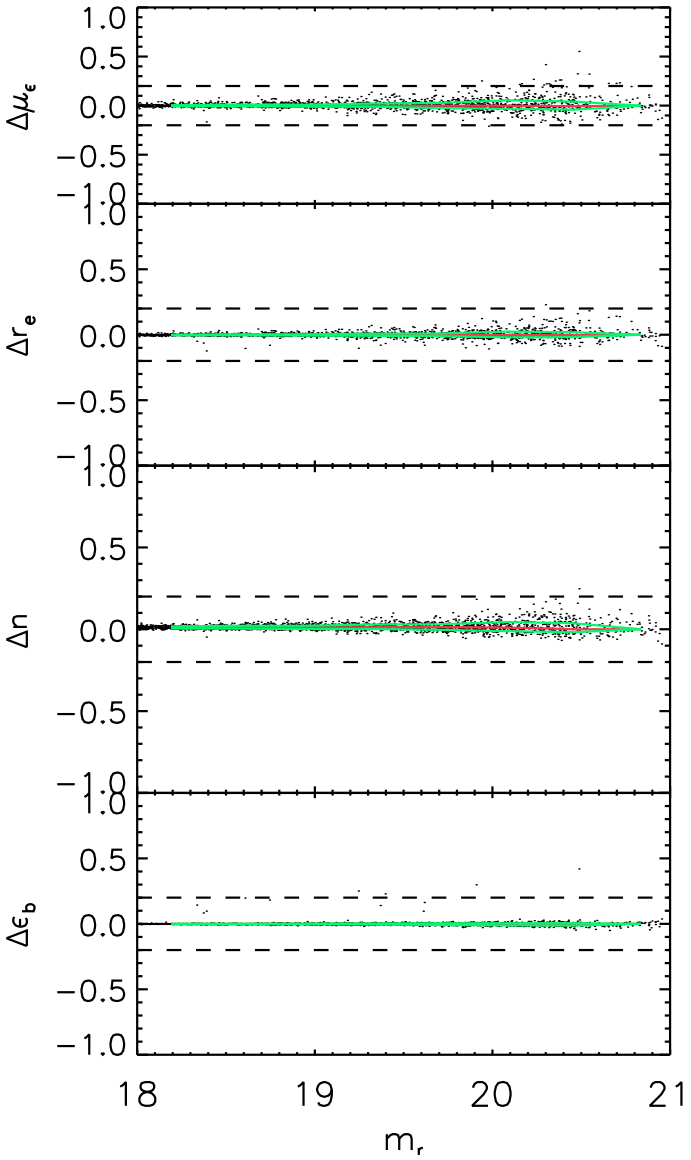

Fig. 1. Magnitudes versus absolute (μ_e) and relative (r_e, n and ϵ_b) errors for the parameters of the Sérsic profile. The horizontal dashed lines are the 20% error. The green (grey) and red (black) lines are the quartile and percentile of the error in bins, respectively.

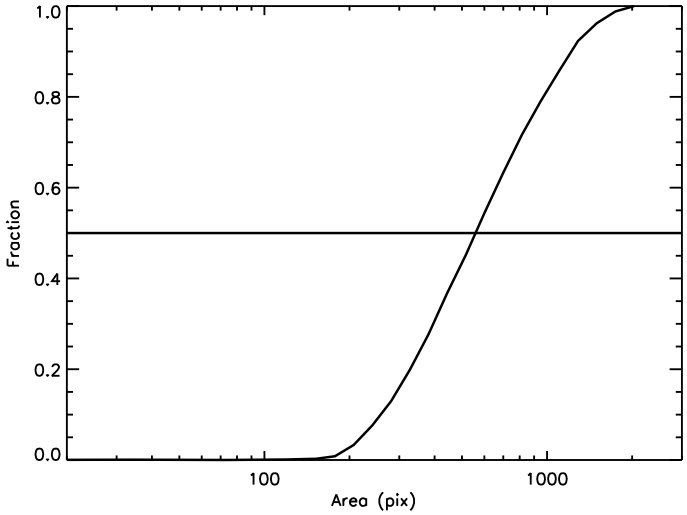

Fig. 2. Fraction of properly fitted galaxies versus area of the one-component simulated galaxies.

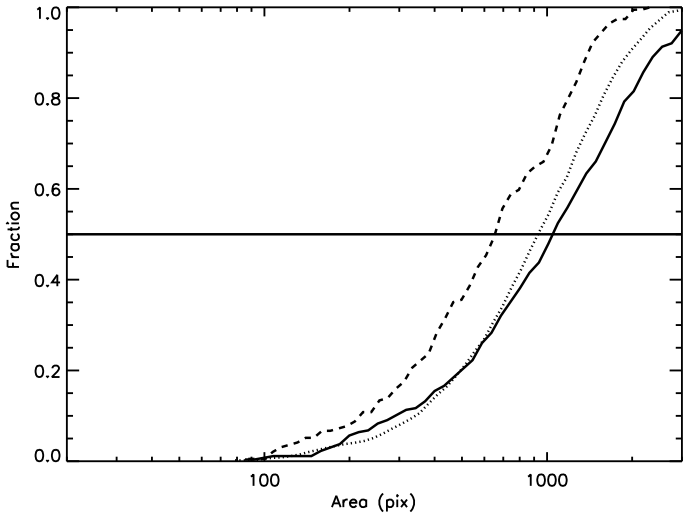

Fig. 3. Fraction of properly fitted bulge and disc simulated galaxies as a function of their area. The full line represents galaxies with $B/T < 0.2$, the dotted line those with $0.2 < B/T < 0.8$, and the dashed line $B/T > 0.8$.

for μ_e and μ_0, where we show the absolute errors. Notice that in general the disc parameters are better fitted than the bulge ones. It is also clear that those galaxies with large B/T show larger errors in the disc parameters than in the bulge ones. In contrast, galaxies with smaller B/T show larger errors in the bulge than in the disc. Indeed, the bulge and disc parameters for faint galaxies ($m_r > 20$) with low surface brightness ($\mu_{0,D} > 25.0$ or $\mu_{0,B} > 25.3$ mag arcsec^{-2}) are not well fitted.

We have also considered that a galaxy was properly fitted if all free parameters were recovered with relative errors smaller than 20%. Figure 3 shows the fraction of properly fitted bulge and disc simulated galaxies. In this case, the area at which at least 50% of the population is well fitted depends on their B/T values. We have adopted in this case 800 pixels as the minimum area in order to obtain reliable fits.

3.3. Number of components

The simulations have shown that all galaxies with areas larger than 800 pixels can be properly fitted. This area corresponds to galaxies brighter than $m_r = 20$. Thus, all the galaxies down to $m_r = 20$ were fitted with one and two components. The galaxies with areas between 550 and 800 pixels were not included in our analysis.

Usually, the χ^2 value is used to decide which is the best fitted model. Nevertheless, models with two components tend to have smaller values of χ^2 than models with one component. This fact is due to the different number of free parameters between both fits. Additionally, it is also possible that the model with the lowest value of χ^2 might not be a physical solution. What is more, luminous, well resolved galaxies with spiral arms or inner dust-lanes that can't be properly described by the model tend to have larger values of χ^2. For these reasons, we have adopted an alternative method in order to decide the best fitted photometric

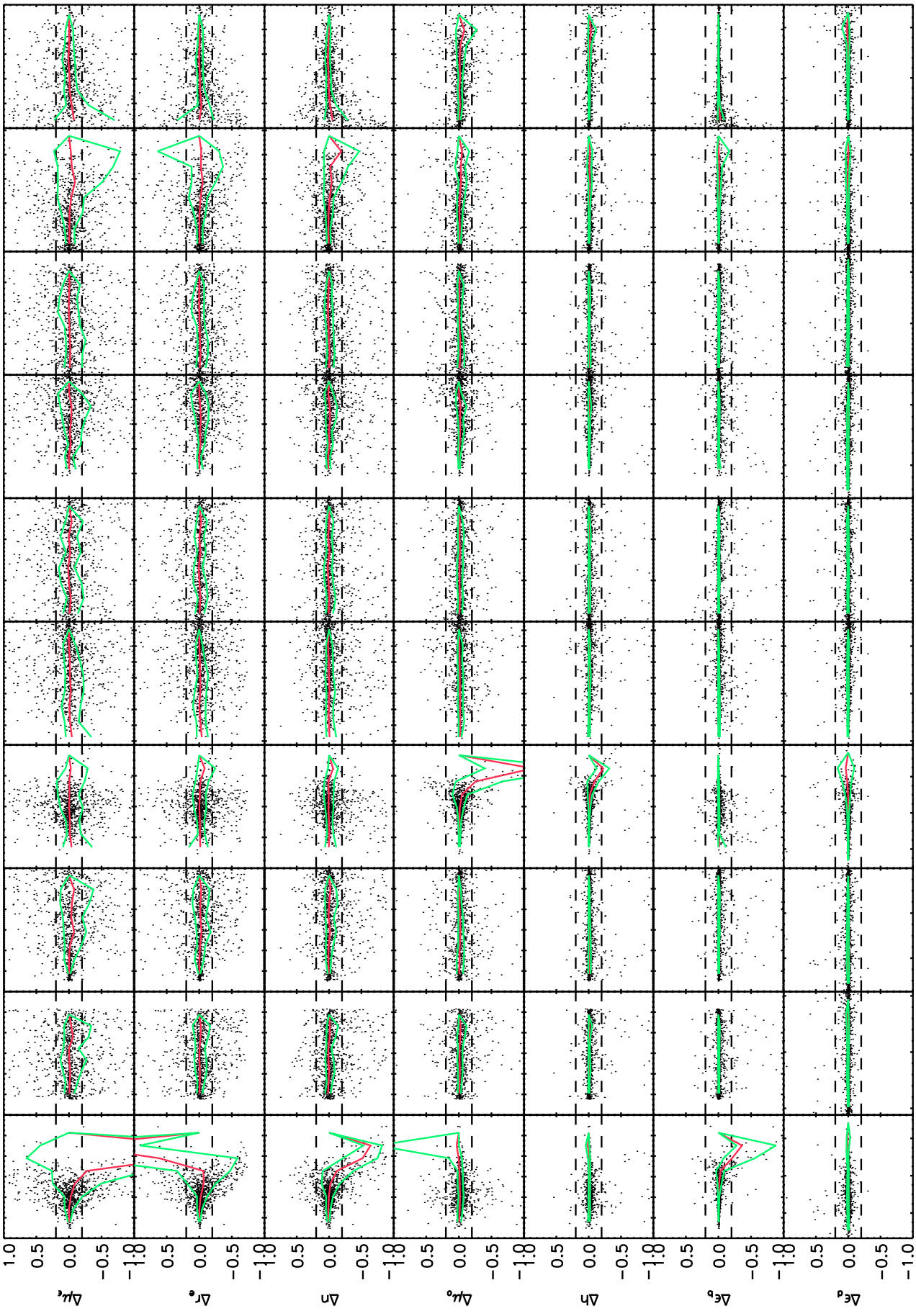

Fig. 4. Sérsic+ Disc profile parameters versus its error for those galaxies with areas larger than 800 pixels (see text for details). The lines are the same as Fig. 1.

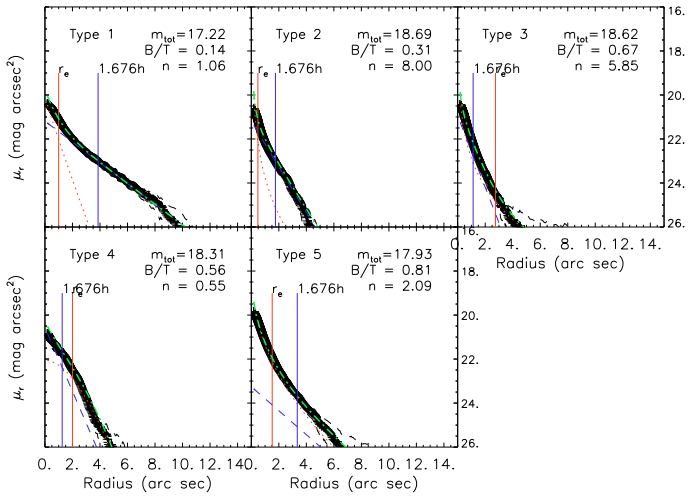

Fig. 5. Examples of profiles 1 to 5 following the notation of Allen et al. (2006). The black solid lines represent the galaxies surface brightness profiles and the black dashed lines show the errors limits. The red dotted lines are the Sérsic profile fits, the blue dashed lines are the disc profile fits and the green dashed dotted lines are the sum of bulge and disc profiles fits.

model. The method is similar to that used by Allen et al. (2006). It is based on the analysis of the surface brightness radial profiles of the fitted models. Our aim is that those galaxies finally fitted with two components should be "classical" bulge and disc systems, i.e. their central regions should be dominated by the bulge component, while the disc dominates at large radial distances from the galaxy center. Galaxies with different light distribution were fitted with only one component.

We have implemented a decision tree algorithm in order to find the best final number of structural components for each galaxy. The algorithm starts by comparing the magnitude of the galaxy obtained from the two component fit and the magnitude measured directly in the image using SExtractor. If the difference between those magnitudes is larger than 0.5 mag, then the galaxy was fitted with only one component (this case only happened for a 2.32% of the galaxies in our sample). This large difference between the modelled and measured magnitudes could be due to several reasons, such as the presence of more than two structural components in the galaxies, or the poor convergence of the fitted method. In the second step of the algorithm, we have analysed the bulge-to-total (B/T) ratio given by the two component fit. Those galaxies clearly dominated by the Sérsic components ($B/T > 0.7$) were also fitted with only one component.

The remaining galaxies were analyzed following a similar procedure as in Allen et al. (2006). We identified five different types of fitted surface brightness profiles (see Fig. 5). According to the number of intersections between the Sérsic and the exponential fitted radial profiles, we can identify those with one (type 1, type 2 and type 4), two (type 3) and zero (type 5) intersections. Type 1 profiles were considered as "classical" bulge plus disc galaxies. The remaining types have different features that make them depart from a classical two component galaxy. Galaxies belonging to type 5 show bulges dominating the whole galaxy. Type 4 galaxies have a disc component dominating in the inner regions of the profile. Type 3 galaxies show a bulge effective radius larger than the disc effective radius ($1.676h$) and type 2 galaxies refer to those galaxies whose Sérsic parameter n has reached the maximum value allowed in the fit.

Eventually, only the galaxies with type 1 profiles were considered as two component fits. The remaining were fitted with only one component. We obtained finally that 47% of the galaxies were fitted with one Sérsic component.

4. Structural parameters

The correlations between the structural parameters of galaxies have been extensively investigated at low redshift in the literature (e.g. De Jong 1996; Graham 2001; Graham 2003; MacArthur et al. 2003; Möllenhoff 2004; Aguerri et al. 2004; Gutiérrez et al. 2004; Aguerri et al. 2005). Our galaxy cluster sample is located at a mean redshift of ∼0.2, and gives us the opportunity to compare the structural parameters of these galaxies with similar ones located in nearby clusters. This comparison will enable us to determine any evolution of the structural parameters of the galaxies in clusters in the last ∼2.5 Gyr.

We have classified the galaxies taking into account the number of fitted photometric components and their $B-r$ colors. Three diferent galaxy types were considered: early-types (E/S0), early-spirals (Spe) and late-spirals (Spe). The results of the fit for the galaxy sample, together with their quantitative classification, are shown in the Table A.1 in the Appendix.

The early-type galaxies were those fitted with one Sérsic component and located in the red sequence of the color-magnitude relations (CMR) of the clusters (within 0.2 magnitudes). Early-type spirals were those fitted with two structural components and also located near the red sequence of the CMR. Late-type spirals were those objects fitted with two components and have at least 0.2 bluer $B - r$ color than the red secuence of the cluster. This classification results in 36%, 29%, and 16% of the galaxies being early-type, early-spirals and late-spirals, respectively. The remaining 19% of the objects correspond to blue galaxies fitted with only one component. These objects could be a mix of different kind of objects (galaxies with more than two galactic components, blue spirals not well fitted with two components, irregular galaxies, blue ellipticals...).

4.1. Sérsic parameters

In the present section we will compare the Sérsic parameters of the galaxies in the sample with similar galaxies located in local galaxy clusters.

Kormendy (1977) discovered a correlation between the size and the surface brightness $\langle\mu_e\rangle$–r_e of elliptical galaxies, the so called, Kormendy Relation. Later on, Binggeli et al. (1984) found that this relationship was only given in elliptical galaxies brighter than $M_B \leq -20$. For fainter galaxies, the tendency inverts.

In Fig. 6, we have plotted the Kormendy relation for E/S0 (red points) and the bulges of Early Spirals (Green triangles). Notice that bulges of early spirals and E/S0 galaxies form a continuous family of objects. The fit of this relation for both types is given by:

$$\langle\mu_e\rangle = (20.32 \pm 0.15) + (2.18 \pm 0.23)\log(r_e). \quad (8)$$

This fit gives that early-type galaxies brighter than $m_r = 20$ in clusters at $z \sim 0.2$ follows the relation $L_V \propto r_e^{1.12\pm0.08}$. This relation is close to that observed for local early-type galaxies, given by $L_B \propto r_e^{1.3}$ (Binggeli et al. 1984).

We have also plotted in Fig. 7 the relation between effective radius and shape parameters for red galaxies fitted with one

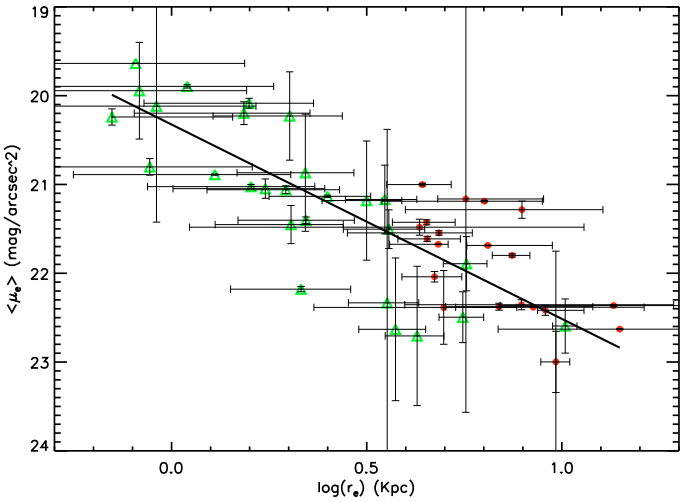

Fig. 6. Kormendy relation between effective ratius and mean bulge surface brightness for the early type sample of galaxies. Red points are E/S0 galaxies and green triangles represent the bulges of the Early Spiral galaxies. The solid line is the fit of the relation.

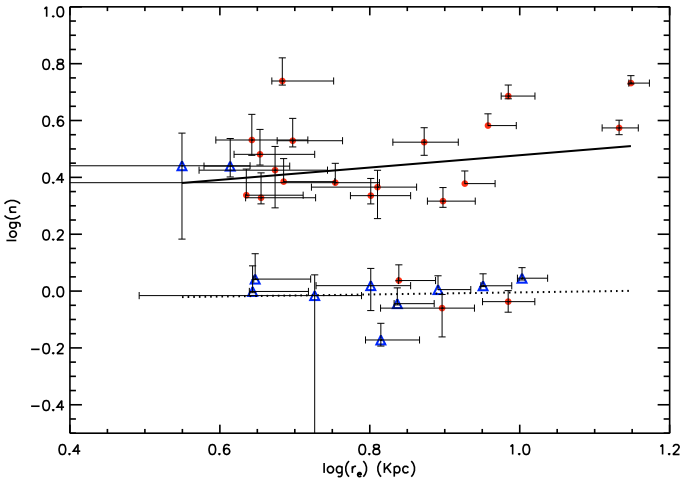

Fig. 7. Relation between effective ratius and shape parameter for one component galaxies. Red points refer to red one component galaxies and blue triangles represent blue one component galaxies. Solid and dotted lines are the respective fits.

component (red points) and blue galaxies fitted with one component (blue triangles). Clearly, a dichotomy exists. By removing the obvious outliers, we have obtained the following fits:

$$\log n = (0.26 \pm 0.13) + (0.21 \pm 0.17)\log(r_e) \quad (9)$$

and for the blue ones

$$\log n = (-0.04 \pm 0.16) - (0.03 \pm 0.19)\log(r_e). \quad (10)$$

These fits are in agreement with recent measurements of the Sérsic indexes in wider samples of galaxies (Driver et al. 2006; Bell 2008) supporting the hypothesis that the origin and formation of these two kinds of galaxies are different. The red and blue population are located in split and parallel regions (within the errors in the slopes) in the $\log(n) - \log(r_e)$ plane. This result allows us to reliably separate the early and late type galaxies by identifying the value of their Sérsic parameter, and inversely, we can assign a particular shape to a galaxy by determining its color. As a consequence, we can conclude that the galaxies fitted with one component have a bimodal behavior. The red early-type galaxy population has an n value of $2 \leq n \leq 4$, while the blue late-type galaxy population has a shape parameter, $n \sim 1$.

We have found two blue galaxies with a Sérsic index similar to the red galaxies in the sample. These galaxies are at 560 kpc distance from the core of A1878, a cluster which in our previous work (Ascaso et al. 2008) was shown to have a large blue fraction as well as a spiral-dominated population. These objects could be blue early-type galaxies results of mergers (Bildfell et al. 2008; Pipino & Matteucci 2008), spiral galaxies with some features such as bars or dust or galaxies in process of merging. As far as the three red galaxies with smaller Sérsic profiles are concerned, one of them is visually classified as spiral, so it might have been classified in one component but is a real spiral galaxy, the two other ones have been classified as ellipticals but a closer inspection of them shows that they are in clear interaction.

Furthermore, in Fig. 8, we have shown the effective surface brightness, the shape parameter and effective radius versus the absolute magnitude (left column) and color (right column) for the E/S0 galaxies (red points) and the bulges of the early spiral galaxies (green triangles). We can see that the $B - r$ colors of

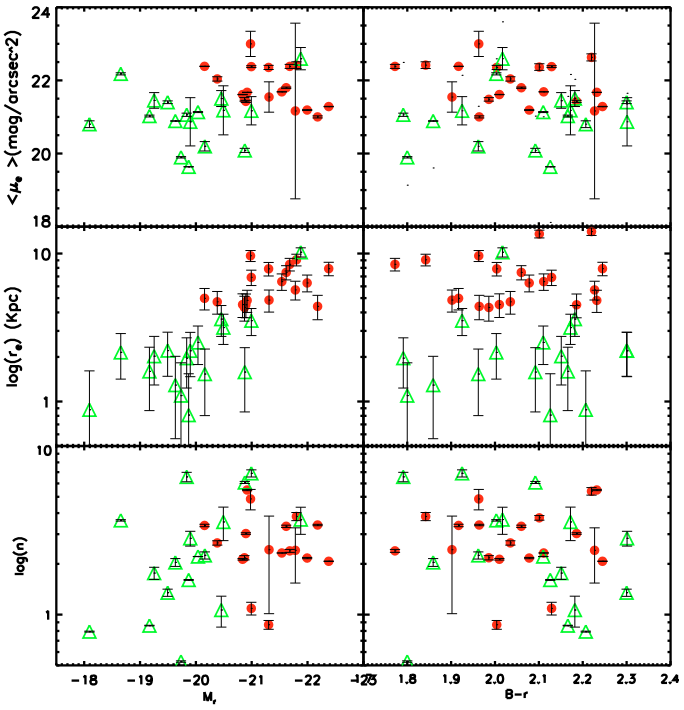

Fig. 8. Absolute Gunn-r magnitude (*left column*) and $B-r$ colour (*right column*) versus $\langle\mu_e\rangle$, n and B/T for E/S0 (red points) and early spirals bulges (green triangles).

bulges of early-type spirals and E/S0 galaxies are similar (median $B - r = 2.04$ and 2.06 respectively). In general, bulges of early-type spiral galaxies show fainter $\langle\mu_e\rangle$ (median value is 21.05 mag arcsec^2), and smaller r_e (median value is 2.02 kpc) and n (median value is 2.21) Sérsic parameters than E/S0 galaxies (median values are 21.79 mag arc sec^2, 6.46 kpc and 2.42 respectively). The plane $\log(r_e) - M_r$ shows a clear continuous relation between early-type bulges and E/S0 galaxies as pointed before by the Kormendy relation.

Table 2. Bulge parameters for the Coma and NOT samples.

Name	$\langle r_e \rangle$	$\sigma(r_e)$	$\langle n \rangle$	$\sigma(n)$	$\langle$Dist (kpc)$\rangle$	σ(Dist (kpc))
NOT	6.58	2.38	2.24	1.35	349.72	257.053
Coma	8.06	16.34	3.49	1.60	410.684	243.904

Finally, we have compared the scales of our E/S0 galaxies with those from similar objects in the Coma cluster (Aguerri et al. 2004). Early-type Coma galaxies were selected as those galaxies with $B/T = 1$ and were fitted with one component. Due to the seeing effect, we have not measured galaxies with scales smaller than 2.2 kpc. For this reason, only galaxies in Coma with $r_e > 2.2$ kpc were considered. We obtained that the sizes of our early-type galaxies turned out to be similar to the Coma cluster galaxies (see Table 2).

As far as the shape parameter is concerned, the range of values in the NOT sample expands all the range of values of Coma. However, we find a mean value somewhat smaller for the NOT sample than for Coma but the values agree within the errors. Therefore, it seems that the bulge sizes have not changed substantially with respect to those in the Coma Cluster.

4.2. Disc parameters

The analysis of the structural parameters of the galaxies in clusters gives information about the role played by the environment in the evolution of galaxies in high density environments. Fast galaxy-galaxy encounters can transform galaxies from late- to early-type in short time-scales (∼1 Gyr). These kinds of encounters are usual in galaxy clusters (Moore et al. 1996). The stars located in galactic discs have a lower binding energy than those located in the central regions of the galaxies. Thus, interactions can strip away easily stars located in the external regions of the galaxies, and truncate the discs. There are hints about this truncation in the literature. Coma cluster galaxies have smaller discs than field nearby galaxies (Gutiérrez et al. 2004; Aguerri et al. 2004). Few facts are known about the evolution of discs at medium redshift in galaxy clusters. In the present section, we have compared the discs of the galaxies located in our medium redshift clusters with similar ones in the local environment.

We have plotted in Fig. 9 the absolute magnitudes of the disks versus their scale parameters. The red diamonds concerns our medium redshift galaxy cluster sample. The blue triangles refer to a sample of field galaxies extracted from Graham (2001) in the R band and the black points are the disks from the Coma cluster taken from Aguerri et al. (2004). The galaxies in the latter sample have been selected as the galaxies with $B/T < 1$ (two component galaxies). There are no discs in the medium redshift clusters with scales $h < 2.4$ kpc. This is due to our minimum cut area (800 pixels) and to the surface brightness limit fitted corresponding to $\mu_r \approx 25.3$ mag arcsec^{-2}. The horizontal dotted line overplotted in Fig. 9 shows this limit.

Our disc scales are as large as those of field galaxies, while those discs in Coma represent a minimum percentage. Figure 9 represents the well known Freeman law (Freeman 1970). The fit of this law for our disk sample is given by:

$$\log h = (-2.52 \pm 0.57) - (0.152 \pm 0.027) M_r.$$

For a quantitative description of the disc scales, we have found that in the central regions of our clusters at medium redshift ($R <$ 200 kpc) there is a population of large disc galaxies that is absent

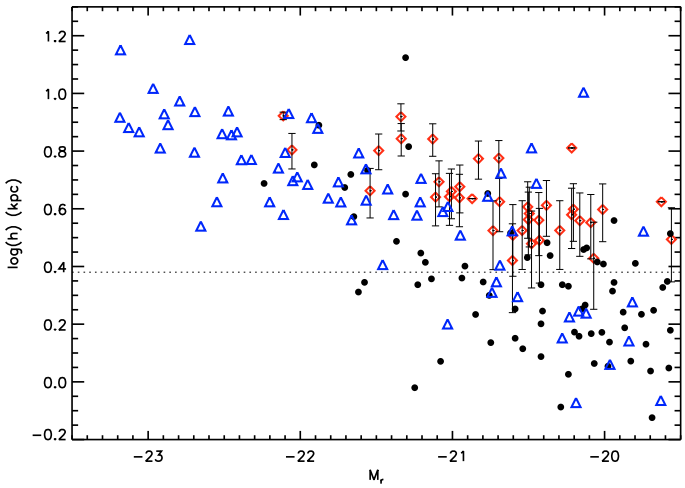

Fig. 9. Disc scales versus absolute Gunn-r Magnitude for two component galaxies (Coma Cluster; Aguerri et al. (2004), black points), NOT sample (red diamonds) and (field galaxies; Graham (2001), blue triangles). The horizontal dotted line shows the minimum disc size determined by the minimum area and surface brightness limit.

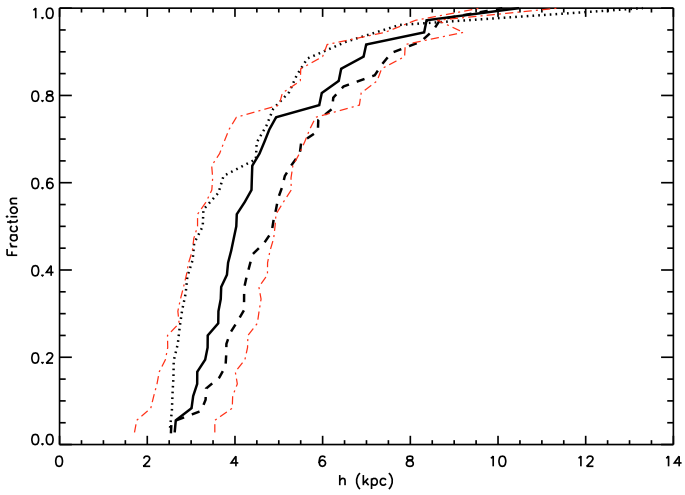

Fig. 10. Cumulative function of disc scales for the NOT sample (solid line), Aguerri et al. (2004) Coma Cluster (dotted line) and Graham (2001) isolated sample (dashed line). The red dotted-dashed lines show the error of the cumulative function for the NOT sample.

in the Coma Cluster as collected in Table 3. These results may agree with an hypothesis of evolution from this range of redshift clusters to the present in the disc scales of the late type galaxy population in clusters.

We have performed statistical tests to check if the disc scales in the NOT medium redshift cluster sample are significantly different to disc scales of nearby galaxies in clusters or in the field. With that purpose, we have run the Kolmogorov-Smirnov (KS) test on the cumulative functions of the disc scales for the clusters in the NOT sample, the Coma sample and the sample of isolated galaxies from Graham (2001). We have selected only galaxies in the same range of magnitudes. These cumulative functions are shown in Fig. 10.

The results of the test suggest that the disc scale distribution of Coma galaxies is statistically different from the disc scale distribution of both our medium redshift clusters (98.1%

Table 3. Disc parameters for the Coma and NOT samples.

Name	$\langle h \rangle$	$\sigma(h)$	$\langle$Dist (kpc)$\rangle$	σ(Dist (kpc))
NOT	4.738	1.941	272.16	202.10
Coma	4.367	2.899	505.008	259.386

significance) and the field galaxy sample (99.9% significance). However, the disc scales of the field galaxy sample and our medium redshift galaxy sample are not statistically different (86.9% significance).

The distributions for Coma and the NOT sample intersect at disc scales of 4 kpc. In Fig. 10, there is a greater difference between the distributions of disc sizes smaller than 4 kpc. We have performed a new Kolmogorov-Smirnov test for galaxies with discs larger than 4 kpc in all samples. The results show that none of the samples can be shown to be statistically different, with 54.95% significance for the Coma Cluster and NOT sample, 28.95% for the Coma Cluster and field galaxy sample and 28.37% for the NOT sample and field galaxy sample.

If we consider in our analysis the galaxies classified visually as spirals in Ascaso et al. (2008), we find similar results. The whole disc scale distribution for Coma and NOT clusters is statistically different with a 98.98% significance, while the NOT clusters and the field galaxy sample are not statistically different (19.41% significance). In addition, by considering only the galaxies with disc scales larger than 4 kpc in this subsample, the disc scales distributions for NOT and Coma galaxy clusters and NOT and field galaxies are not statistically different, with 66.55% and 28.95% respectively. This result reinforces the difference in the smaller disc scale distributions in local and medium redshift clusters from a morphological point of view.

Thus, Coma shows an excess of galaxies with disc scales smaller than 4 kpc with respect to the field galaxy and NOT sample. Field galaxies with large discs could have entered the cluster and undergone interactions with the environment that have made the discs become smaller (Aguerri et al. 2005; Aguerri & González-García 2009; Kormendy et al. 2009) in the last 2.5 Gyr. This conclusion supports a scenario in which the environment plays a crucial role in galaxy evolution.

5. Discussion and conclusions

In this paper, we have analyzed the structural properties of a sample of galaxies placed in five clusters between $0.18 \leq z \leq 0.25$. The structural parameters derived from this quantitative classification have shown that the galaxies fitted with one component have a nearly univocally correspondence with the shape parameter. Red galaxies fitted with one component have a shape parameter between 2 and 4, while for the blue galaxies fitted with one component, the shape parameter we obtain is around 1. This bi-modality has been already observed in previous works (Driver et al. 2006; Bell 2008), showing a clear difference in the formation and evolution of these two types of galaxy population.

Likewise, we have examined the relation of the structural parameters. We have tested the Kormendy Relation and we have found that the E/S0 and the bulges of early spirals seem to be a continuous set of parameters. Similar results are obtained with magnitude and color in Fig. 8. The results show that r_e and n follow a correlation with the magnitude taking out the obvious outliers for the early types and for the bulges of early spirals, suggesting a similar nature of these objects.

On the other hand, we have compared the bulge scales of the galaxies in the sample with the scale of the bulges of galaxies in the Coma cluster (Aguerri et al. 2004), obtaining the same range of values. We have compared the disc scales of the galaxies in our medium redshift sample with the disc scales in a sample of galaxies in Coma studied by Aguerri et al. (2004) and the disc scales of a sample of local field galaxies studied by Graham (2001). We considered the whole galaxy sample classified in two components following the procedure explained in 3.3 and also, to make sure that we were comparing spiral visually classified galaxies, we took the whole galaxy sample classified as spiral galaxies in Ascaso et al. (2008). We found in both cases that the disc scales of the galaxies in our sample are slightly larger than those in the Coma cluster and are statistically different. Moreover, the distribution of disc scales for the NOT sample is not statistically different to the disc scales for the local field galaxies This result indicates an evolution in the disc scales of the galaxies in clusters at medium redshift from local clusters.

Interestingly, we have seen that the main difference in the distribution is concentrated in the small disc galaxies (<4 kpc). This implies a different behavior of small and large disc galaxies, indicating the different nature of these kinds of objects. There is a large population of galaxies with $h < 4$ kpc in the Coma cluster not observed in the field or in the medium redshift clusters.

One of the main concerns in the present work is that the compared galaxy clusters at $z \sim 0$ (the Coma cluster) and at $z \sim 0.25$ (our NOT sample) are not statistically complete samples. It can be argued that the Coma cluster is not a representative comparison due to its high mass and degree of evolution. Thus, the different disc scales found between the Coma cluster and those at medium redshift could be due to the fact that we are comparing clusters with very different properties. We have tested this assumption by splitting our cluster sample into two groups according to their galaxy richness: poor clusters (Richness Class (RC) < 2) and rich clusters ($RC \geq 2$). The Coma cluster has a richness class similar to our rich cluster sample at $z \sim 0.25$ ($RC = 2$). We have found that, for both samples, their disc scale length distributions are different to Coma and similar to the field one. This same tendency is observed for the overall distribution. Therefore, the result does not depend on the richness of the clusters.

More work needs to be done in the future to span both cluster samples and determine the variance in the disc scale distribution in nearby and medium redshift clusters. Nevertheless, this result indicates that there was a strong evolution in the external parts of the galaxies in these clusters during the last 2.5 Gyr, or that Coma is in some way anomalous. Mechanisms such us galaxy harassment with small timescales (∼1 Gyr) could explain this evolution.

Acknowledgements. We acknowledge the anonymous referee for improving this paper. BA is partially supported by NASA grant NNG05GD32G. JALA and RSJ were partially supported by the Ministerio de Ciencia e innovación by the grants AYA2007-67965-C03-01 and CSD2006-00070.

Appendix A

Table A.1. Results of the 2-dimensional surface brightness fit for the galaxies in the NOT sample

Name	α (J2000) h:m:s	δ (J2000) d:m:s	z	$B-r$	M_r	μ_e mag/arc sec^2	r_e arc sec	e_b	μ_0 mag/arc sec^2	h arc sec	e_d	n	PA$_b$	PA$_d$	B/T	χ^2	Col	T
A 1643	12:55:55.18	44:03:47.50		2.013	–20.67	24.06	1.15597	0.739	21.14	1.10000	0.586	8.000	169.217	11.828	0.324	2.308	*R*	S0
A 1643	12:55:47.93	44:04:01.20		2.035	–20.36	22.91	1.45499	0.756	0.00	0.00000	0.000	2.663	0.087	0.000	1.000	1.089	*R*	E
A 1643	12:55:50.96	44:04:31.00		1.930	–21.15	21.13	0.217008	0.449	21.20	1.46502	0.775	8.000	137.578	41.868	0.065	2.168	*R*	E
A 1643	12:55:55.35	44:04:34.40		1.963	–20.69	24.49	2.97792	1.000	0.00	0.00000	0.000	4.854	88.788	0.000	1.000	3.292	*R*	E
A 1643	12:55:52.70	44:04:44.50		1.818	–20.42	23.10	1.31296	0.285	21.34	0.962016	0.564	8.000	57.503	50.222	0.485	1.915	*R*	S0
A 1643	12:55:59.29	44:04:57.10		2.011	–20.02	23.02	2.97704	0.192	0.00	0.00000	0.000	0.918	126.466	0.000	1.000	2.328	*R*	S
A 1643	12:55:54.00	44:05:12.40		2.060	–21.61	22.69	2.29997	0.691	0.00	0.00000	0.000	3.341	1.579	0.000	1.000	1.515	*R*	S0
A 1643	12:55:45.24	44:06:34.00		2.301	–21.74	21.64	0.679008	0.670	22.06	2.56203	0.793	2.835	12.302	46.929	0.210	1.628	*R*	S
A 1643	12:55:33.82	44:07:12.50		2.186	–20.93	22.53	1.38899	0.879	0.00	0.00000	0.000	3.027	108.131	0.000	1.000	2.479	*R*	E
A 1643	12:55:36.40	44:07:53.40		1.017	–20.71	22.56	2.75598	0.318	0.00	0.00000	0.000	1.044	67.353	0.000	1.000	7.040	*B*	I
A 1643	12:55:36.57	44:08:30.40		1.917	–20.27	23.47	1.53595	0.819	0.00	0.00000	0.000	3.380	12.872	0.000	1.000	1.532	*R*	E
A 1878	14:12:47.82	29:13:53.40		2.111	–21.69	22.06	1.83603	0.508	0.00	0.00000	0.000	2.321	0.688	0.000	1.000	3.025	*R*	S
A 1878	14:12:49.47	29:14:09.90		2.151	–21.57	21.43	0.574992	0.404	20.89	1.24203	0.807	1.763	70.882	20.411	0.145	1.341	*R*	S
A 1878	14:12:52.50	29:14:11.40		1.701	–20.94	22.03	1.25101	0.725	0.00	0.00000	0.000	0.997	49.960	0.000	1.000	2.567	*B*	S
A 1878	14:12:54.15	29:14:19.30		2.207	–20.80	20.89	0.249920	0.633	20.82	0.880000	0.807	0.793	22.695	34.053	0.099	1.132	*R*	E
A 1878	14:12:52.18	29:14:28.40	0.2220	2.300	–22.36	21.35	0.627968	0.441	20.71	1.80998	0.770	1.350	45.974	1.528	0.081	2.285	*R*	E
A 1878	14:12:46.85	29:14:26.40		1.655	–21.02	22.47	1.85504	0.554	0.00	0.00000	0.000	0.673	82.918	0.000	1.000	2.476	*B*	I
A 1878	14:12:54.72	29:14:31.90		2.172	–21.42	22.16	0.897952	0.726	21.24	1.14893	0.745	3.544	34.265	62.113	0.481	1.199	*R*	E
A 1878	14:12:50.98	29:14:42.30		2.003	–20.84	22.59	0.610016	0.425	21.51	1.16301	0.835	3.623	167.017	31.290	0.160	1.736	*R*	I
A 1878	14:12:49.12	29:14:42.50		2.135	–21.38	24.25	1.58400	1.000	20.57	1.19698	0.438	8.000	63.119	38.637	0.420	2.355	*R*	S
A 1878	14:12:50.96	29:14:56.60		2.166	–21.29	21.56	0.454080	0.918	20.99	1.68802	0.369	0.861	147.586	4.530	0.169	1.703	*R*	S
A 1878	14:12:46.58	29:14:59.10		2.280	–20.94	23.28	1.01394	0.476	20.57	0.951984	0.481	8.000	160.326	48.481	0.332	1.774	*R*	S0
A 1878	14:12:52.43	29:15:48.70		2.212	–21.00	20.88	0.259952	0.402	20.32	0.915024	0.550	8.000	8.221	59.070	0.159	1.789	*R*	S0
A 1878	14:13:00.54	29:13:56.90		1.771	–21.15	23.67	1.46397	0.812	21.47	1.12499	0.610	5.988	143.886	133.731	0.582	1.324	*B*	S0
A 1878	14:12:57.80	29:12:01.60		1.508	–20.47	22.77	1.26104	0.911	0.00	0.00000	0.000	1.102	114.178	0.000	1.000	3.744	*B*	S0
A 1878	14:12:59.05	29:12:14.40		1.611	–20.60	22.26	1.00707	0.697	0.00	0.00000	0.000	2.759	177.224	0.000	1.000	2.358	*B*	E
A 1878	14:12:59.84	29:12:19.50		1.750	–20.45	21.68	1.12006	0.065	23.00	2.97106	0.214	2.400	53.622	52.732	0.305	4.800	*B*	S
A 1878	14:13:00.58	29:12:22.90		1.368	–20.30	22.99	1.51395	0.661	0.00	0.00000	0.000	0.964	145.345	0.000	1.000	2.068	*B*	S
A 1878	14:13:05.59	29:12:54.20		1.675	–20.53	21.89	0.815056	0.428	21.50	1.02907	0.864	1.152	111.972	61.071	0.318	1.645	*B*	E
A 1878	14:13:02.81	29:12:55.70		1.869	–19.44	22.01	1.16794	0.393	0.00	0.00000	0.000	2.751	135.302	0.000	1.000	3.636	*B*	S
A 1952	14:41:07.84	28:38:29.40		2.102	–22.05	23.20	1.47893	0.662	20.61	1.64402	0.774	8.000	16.433	53.677	0.402	1.129	*R*	E
A 1952	14:41:01.92	28:37:14.50		2.126	–20.76	18.11	0.209968	0.105	20.24	0.696080	0.838	1.606	104.714	74.489	0.285	0.955	*R*	E
A 1952	14:41:02.66	28:37:10.00		2.220	–22.11	23.84	3.65200	0.734	0.00	0.00000	0.000	5.391	29.119	0.000	1.000	1.835	*R*	S0
A 1952	14:41:03.13	28:37:10.10		1.964	–21.41	22.12	1.13995	0.843	0.00	0.00000	0.000	3.400	108.770	0.000	1.000	1.795	*R*	E
A 1952	14:41:01.19	28:37:00.50		2.061	–21.20	21.51	0.520960	0.649	20.07	0.947936	0.575	8.000	21.700	61.873	0.489	0.924	*R*	E
A 1952	14:41:01.32	28:37:43.20		2.092	–21.57	21.02	0.410080	0.536	20.63	1.28198	0.902	6.079	156.086	73.545	0.282	0.780	*R*	E
A 1952	14:41:13.59	28:37:29.60		1.786	–22.13	22.45	1.51800	0.742	19.59	1.12798	0.395	4.693	157.794	140.539	0.666	1.639	*B*	S0
A 1952	14:41:14.94	28:37:42.60		1.877	–21.80	20.44	0.677072	0.590	20.77	1.80400	0.536	1.200	68.440	79.062	0.475	1.825	*B*	S0
A 1952	14:41:07.59	28:35:35.00		1.733	–21.58	21.86	2.61395	0.211	0.00	0.00000	0.000	1.110	98.621	0.000	1.000	13.768	*B*	S
A 1952	14:41:08.19	28:35:44.50		1.567	–21.61	22.46	1.05406	0.404	20.49	1.18694	0.860	6.009	28.048	28.236	0.356	3.480	*B*	S0
A 1952	14:41:07.03	28:36:39.20		0.504	–22.10	16.91	0.186912	0.308	19.86	0.781968	0.681	2.343	168.989	83.230	0.696	7.501	*B*	S0
A 1952	14:41:03.11	28:36:46.60		1.859	–20.74	19.60	0.334928	0.117	20.41	0.994928	0.704	2.041	96.391	88.057	0.178	1.366	*R*	S0
A 1952	14:41:03.57	28:37:00.30		2.101	–22.61	23.65	3.52194	0.937	0.00	0.00000	0.000	3.750	105.293	0.000	1.000	1.711	*R*	E
A 1952	14:41:08.25	28:37:13.80		1.676	–21.85	20.84	0.687984	0.604	20.38	1.13802	0.803	2.041	49.162	106.764	0.482	3.233	*B*	S
A 2111	15:39:37.64	34:27:03.80	0.2295	2.110	–21.26	21.00	0.690976	0.326	20.99	0.922944	0.810	2.211	20.762	24.650	0.375	1.441	*R*	S0
A 2111	15:39:40.49	34:25:27.30	0.2282	2.182	–22.67	22.02	0.992992	0.830	21.21	2.30402	0.672	1.065	174.278	41.050	0.172	1.530	*R*	E
A 2111	15:39:39.20	34:25:11.50		2.129	–21.13	22.85	1.90098	0.787	0.00	0.00000	0.000	1.089	83.748	0.000	1.000	7.623	*R*	E

Table A.1. continued.

Name	α (J2000) h:m:s	δ (J2000) d:m:s	z	$B-r$	M_r	μ_e mag/arcsec^2	r_e arcsec	e_b	μ_0 mag/arcsec^2	h arcsec	e_d	n	PA$_b$	PA$_d$	B/T	χ^2	Col	T
A 2111	15:39:39.39	34:25:13.40	0.2211	2.004	–21.34	22.78	2.17096	0.831	0.00	0.00000	0.000	0.871	20.000	0.000	1.000	5.658	*R*	E
A 2111	15:39:36.79	34:25:39.10	0.2312	2.232	–20.90	22.41	1.32898	0.469	0.00	0.00000	0.000	5.484	4.038	0.000	1.000	4.855	*R*	S0
A 2111	15:39:34.26	34:26:12.50	0.2289	2.227	–21.97	22.12	1.56394	0.859	0.00	0.00000	0.000	2.406	134.942	0.000	1.000	3.430	*R*	S0
A 2111	15:39:38.70	34:26:38.80	0.2246	1.477	–20.85	22.20	1.89200	0.311	0.00	0.00000	0.000	0.903	20.000	0.000	1.000	2.158	*B*	S
A 2111	15:39:41.34	34:24:34.30	0.2294	2.111	–20.97	22.11	0.479072	0.528	21.21	1.04597	0.569	8.000	178.202	62.997	0.296	1.561	*R*	S
A 2111	15:39:41.81	34:24:42.70	0.2292	2.245	–22.61	22.25	2.17694	0.929	0.00	0.00000	0.000	2.072	142.212	0.000	1.000	1.469	*R*	E
A 2111	15:39:47.09	34:27:37.90	0.2368	1.666	–21.25	21.49	0.652960	0.268	20.70	0.922064	0.735	2.042	153.304	143.414	0.184	1.712	*B*	S0
A 2111	15:39:52.99	34:27:48.60	0.2297	2.010	–20.98	21.85	1.24502	0.468	0.00	0.00000	0.000	2.130	81.730	0.000	1.000	2.925	*R*	S0
A 2111	15:39:42.02	34:26:30.30	0.2258	2.078	–22.09	22.23	1.74398	0.975	0.00	0.00000	0.000	2.166	10.666	0.000	1.000	0.869	*R*	E
A 2111	15:39:49.35	34:26:41.50	0.2299	1.548	–21.54	22.38	1.74398	0.734	0.00	0.00000	0.000	1.045	14.595	0.000	1.000	4.741	*B*	S
A 2111	15:39:45.75	34:26:57.40	0.2292	1.965	–21.07	18.86	0.227920	0.255	20.57	0.726000	0.936	0.500	49.420	54.609	0.156	1.207	*R*	E
A 2111	15:39:52.15	34:27:12.20		1.050	–21.13	23.31	2.14403	0.728	0.00	0.00000	0.000	1.012	35.048	0.000	1.000	1.646	*B*	S
A 2111	15:39:47.34	34:25:10.20	0.2309	1.986	–21.07	22.47	1.18994	0.924	0.00	0.00000	0.000	2.174	126.333	0.000	1.000	1.065	*R*	E
A 2658	23:44:50.35	–12:18:25.50		1.800	–21.89	19.13	0.356928	0.335	20.00	1.49706	0.656	0.527	97.394	55.478	0.115	8.090	*R*	S
A 2658	23:44:46.97	–12:18:10.40		1.962	–20.94	21.29	0.498960	1.000	20.81	1.29202	0.545	2.246	134.927	160.502	0.398	4.597	*R*	S0
A 2658	23:44:54.27	–12:17:59.30		1.925	–21.42	22.13	1.14594	0.520	20.71	1.18395	0.727	6.887	21.717	75.161	0.536	6.948	*R*	E
A 2658	23:44:47.44	–12:17:47.40		1.902	–20.92	22.51	1.57696	0.862	0.00	0.00000	0.000	2.427	69.348	0.000	1.000	4.363	*R*	E
A 2658	23:44:50.26	–12:17:20.90		1.842	–21.07	23.36	2.95398	0.679	0.00	0.00000	0.000	3.821	31.148	0.000	1.000	3.693	*R*	S0
A 2658	23:44:49.84	–12:17:26.70		1.791	–21.32	22.49	0.639056	0.815	21.60	1.94304	0.784	6.561	41.131	29.707	0.238	5.542	*R*	E
A 2658	23:44:49.80	-12:17:39.50		2.017	–22.39	23.60	3.32094	0.731	21.34	2.26794	0.814	3.665	10.701	61.252	0.531	3.578	*R*	E
A 2658	23:44:56.18	–12:17:07.50		1.772	–21.14	23.14	2.75106	0.719	0.00	0.00000	0.000	2.388	11.523	0.000	1.000	11.770	*R*	S

Note. Col. (1): Galaxy Cluster; Col. (2): Right ascension (J2000); Col. (3): Declination (J2000); Col. (4): Redshift; Col. (5): $B-r$ color; Col. (6): Gunn-r Absolute magnitude; Col. (7): Effective surface brightness of the bulge; Col. (8): Effective radius of the bulge; Col. (9): Ellipticity of the bulge; Col. (10): Central surface brightness of the disk; Col. (11): Scale length of the disk; Col. (12): Ellipticity of the disk; Col. (13): Shape parameter of the bulge; Col. (14): Position angle of the bulge; Col. (15): Position angle of the disk; Col. (16): bulge-to-total luminosity ratio; Col. (17): χ^2 of the fit; Col. (18): Assigned color. Red (*R*) galaxies are located within 0.2 mag from the CMR of the host cluster and Blue (*B*) galaxies are bluer than 0.2 mag the CMR of the cluster; Col. (19): Visual morphological type extracted from Ascaso et al. (2008).

References

Aguerri, J. A. L., & González-García, A. C. 2009, A&A, 494, 891
Aguerri, J. A. L., Balcells, M., & Peletier, R. F. 2001, A&A, 367, 428
Aguerri, J. A. L., Iglesias-Páramo, J., Vilchez J. M., & Munoz-Tunón, C., 2004, ApJ, 127, 1344
Aguerri, J. A. L., Iglesias-Páramo, J., Vílchez, J. M., Muñoz-Tuñón, C., & Sánchez-Janssen, R. 2005, AJ, 130, 475
Allen, P. D., Driver, S. P., Graham, A. W., et al. 2006, MNRAS, 371, 2
Amorin, R. O., Muñoz-Tuñón, C., Aguerri, J. A. L., Cairós, L. M., & Caon, N. 2007, A&A, 467, 541
Amorín, R., Aguerri, J. A. L., Muñoz-Tuñón, C., & Cairós, L. M. 2009, A&A, 501, 75
Andredakis, Y. C., Peletier, R. F., & Balcells, M. 1995, MNRAS, 275, 874
Ascaso, B. 2008, Tesis Doctoral, Universidad de Granada
Ascaso, B., Moles, M., Aguerri, J. A. L., Sánchez-Janssen, R., & Varela, J. 2008, A&A, 487, 453
Balogh, M., Bower, R. G., Smail, I., et al. 2002, MNRAS, 337, 256
Bekki, K., Couch, W. J., & Shioya, Y. 2002, ApJ, 577, 651
Bell, E. F. 2008, ApJ, 682, 355
Bildfell, C., Hoekstra, H., Babul, A., & Mahdavi, A. 2008, MNRAS, 389, 1637
Binggeli, B., & Jerjen, H. 1998, A&A, 333, 17
Binggeli, B., Sandage, A., & Tarenghi, M. 1984, AJ, 89, 64
Bower, R. G., Kodama, T., & Terlevich, A. 1998, MNRAS, 299, 1193
Cameron, E., & Driver, S. P. 2009, A&A, 493, 489
Caon, N., Capaccioli, M., & D'Onofrio, M., 1993, MNRAS, 265, 1013
Caon, N., Cairós, L. M., Aguerri, J., Alfonso, L., & Muñoz-Tuñón, C. 2005, ApJS, 157, 218
de Jong, R. S. 1996, A&A, 313, 45
De Lucia, G., & Blaizot, J. 2007, MNRAS, 375, 2
Desai, V., Dalcanton, J. J., Aragón-Salamanca, A. 2007, ApJ, 660, 1151
Dressler, A. 1980, ApJ, 236, 351
Dressler, A., Oemler, A., Jr., Couch, W. J., et al. 1997, ApJ, 490, 577
Driver, S. P., Allen, P. D., Graham, A. W., et al., 2006, MNRAS, 368, 414
Eliche-Moral, M. C., Balcells, M., Aguerri, J. A. L., & González-García, A. C. 2006, A&A, 457, 91
Fasano, G., Poggianti, B., Couch, W. J., et al. 2000, A&A, 542, 673
Freeman, K. C. 1970, ApJ, 160, 811
Gadotti, D. A. 2008, MNRAS, 384, 420
Graham, A. W. 2001, AJ, 121, 820
Graham, A. W. 2003, AJ, 125, 3398
Graham, A. W., & Driver, S. P. 2005, Publications of the Astronomical Society of Australia, 22, 118
Graham, A. W., & Guzman 2003, AJ, 125, 2936
Gunn, J. E., & Gott, J. R. I. 1972, ApJ, 176, 1
Gutiérrez, C. M., Trujillo, I., Aguerri, J. A. L., Graham, A. W., & Caon, N. 2004, ApJ, 602, 664
Jørgensen, I., & Franx, M. 1994, ApJ, 433, 553
Jørgensen, I., Franx, M. & Kjaergaard, P. 1996, MNRAS, 280, 167
Kauffmann, G., Guiderdoni, B., & White, S. D. M. 1994, MNRAS, 267, 981
Kormendy, J. 1977, ApJ, 217, 406
Kormendy, J., Fisher, D. B., Cornell, M. E., & Bender, R. 2009, ApJS, 182, 216
Krajnović, D., Bacon, R., Cappellari, M., et al. 2008, MNRAS, 390, 93
MacArthur, L. A., Courteau, S., & Holtzman, J. A. 2003, ApJ, 582, 689
Méndez-Abreu, J., Aguerri, J. A. L., Corsini, E. M., & Simonneau, E. 2008, A&A, 478, 353
Merritt, D. 1984, ApJ, 276, 26
Möllenhoff, C. 2004, A&A, 415, 63
Moore, B., Katz, N., Lake, G., Dressler, A., & Oemler, A. 1996, Nature, 379, 613
Pipino, A., & Matteucci, F. 2008, A&A, 486, 763
Postman, M., Franx, M., Cross, N. J. G., et al. 2005, ApJ, 623, 721
Press, W. H., Teukolsky, S. A., Vetterling, W. T., & Flannery, B. P., et al. 1992, Numerical recipes in FORTRAN: The art of Scientic Computing (Cambridge: Cambridge Univ. Press)
Prieto, M., Aguerri, J. A. L., Varela, A. M., & Muñoz-Tuñón, C., et al. 2001, A&A, 367, 405
Quilis, V., Moore, B., & Bower, R. 2000, Science, 288, 1617
Sandage, A., & Visvanathan, N. 1978, ApJ, 225, 742
Sérsic, J. L. 1968, Atlas de Galaxias Australes (Córdoba: Obs. Astron. Univ. Nac. Córdoba)
Skibba R. A., Bamford, S. P., Nichol, R. C., et al. 2009, MNRAS, 399, 966
Trujillo, I., & Aguerri, J. A. L. 2004, MNRAS, 355, 82
Trujillo, I., Aguerri, J. A. L., Cepa, J., & Gutiérrez, C. M. 2001, MNRAS, 328, 977